Biochemistry

 Volume 34, Number 51 December 26, 1995

Articles

Coordination of the Rieske-Type [2Fe-2S] Cluster of the Terminal Iron−Sulfur Protein of *Pseudomonas putida* Benzene 1,2-Dioxygenase, Studied by One- and Two-Dimensional Electron Spin-Echo Envelope Modulation Spectroscopy†

Jasvinder K. Shergill,* Christopher L. Joannou,‡ Jeremy R. Mason, and Richard Cammack

Center for the Study of Metals in Biology and Medicine, Division of Life Sciences, King's College, University of London, Campden Hill Road, London W8 7AH, U.K.

Received August 7, 1995; Revised Manuscript Received October 18, 1995®

ABSTRACT: One- and two-dimensional (1D and 2D) electron spin-echo envelope modulation (ESEEM) spectroscopy has been used to investigate the ligand environment of the [2Fe-2S] cluster from the terminal dioxygenase (ISP_{BED}) of the *Pseudomonas putida* benzene dioxygenase complex. The modulation frequencies observed in the 0.5−8.5 MHz region of the Fourier transforms of 1D and 2D ESEEM spectra measured across the electron paramagnetic resonance (EPR) absorbance envelope (from g_z through to g_x) are consistent with their assignment to two ^{14}N nuclei. Using hyperfine sublevel correlation spectroscopy (HYSCORE), two sets of correlated double quantum transitions sharing the same hyperfine coupling were observed and were identified as being due to the same two ^{14}N nuclei. On the basis of the isotropic hyperfine and quadrupolar couplings estimated for these ^{14}N nuclei [N(1), A_{iso} = 3.6 MHz and e^2qQ = 2.2−2.8 MHz; N(2), A_{iso} = 4.8 MHz and e^2qQ = 2.2−2.4 MHz], the ESEEM pattern of ISP_{BED} is assigned to two histidine nitrogens which are directly coordinated to the reduced iron−sulfur cluster. Bonding parameters of the two [^{14}N]histidine ligands were calculated from these hyperfine couplings. The primary covalent contributions to the hyperfine interaction arise from ^{14}N-to-Fe^{2+} σ bonds. For N(1), our analysis of the percentage of unpaired 2s and 2p electrons gave $f_{2s} \sim 1.3\%$ and $f_{2p} \sim 0.2\%$, while values of $f_{2s} \sim 1.7\%$ and $f_{2p} \sim 1.4\%$ were estimated for N(2). Comparison of these values with those determined from electron nuclear double resonance (ENDOR) data of the Rieske-type [2Fe-2S] center of *Pseudomonas cepacia* phthalate dioxygenase [Gurbiel, R. J., Batie, C. J., Sivaraja, M., True, A. E., Fee, J. A., Hoffman, B. M., & Ballou, D. P. (1989) *Biochemistry 28*, 4861−4871] indicates an apparent reduction in unpaired electron spin density residing on the two ^{14}N ligands of ISP_{BED}. Analysis of slices of the HYSCORE spectrum has provided evidence for another ^{14}N nucleus ($A \sim 1.1$ MHz, e^2qQ = 3.3 MHz), which we have attributed to a weakly coupled peptide nitrogen, similar to those observed for ferredoxin-type [2Fe-2S] clusters. This type of weak interaction has not been previously described by the detailed ENDOR and ESEEM studies of Rieske-type centers. The resolution of the spectra demonstrates the effectiveness of 2D ESEEM for the disentanglement of multiple hyperfine interactions to metalloprotein centers.

Benzene dioxygenase (EC 1.14.12.3) from *Pseudomonas putida* ML2 catalyzes the introduction of two hydroxyl groups into the aromatic nucleus of benzene, resulting in the formation of *cis*-benzene dihydrodiol (Gibson & Sub-

† This work was supported by grants from the United Kingdom Science and Engineering Council (GR/J00151) and Shell Research Ltd.

* To whom correspondence should be addressed.

‡ Present address: Department of Biochemistry, Guy's Hospital, St. Thomas's Street, London SE1 9RT, UK.

® Abstract published in *Advance ACS Abstracts,* December 1, 1995.

0006-2960/95/0434-16533$09.00/0

ramanian, 1984; Mason & Cammack, 1992). For hydroxylation of the benzene ring to occur, benzene dioxygenase requires both oxygen and Fe^{II} to be present. ISP_{BED},[1] the catalytic iron−sulfur protein component of the dioxygenase enzyme, is a large protein (M_r = 146.7 KDa) consisting of two dissimilar subunits arranged in an $\alpha_2\beta_2$ configuration and is often referred to as the terminal dioxygenase. In addition to an iron-binding site, it also contains one [2Fe-2S] cluster per $\alpha\beta$ dimer, located in the α subunit (Butler, 1995). In the classification of Batie et al. (1991), benzene dioxygenase is classed as a three-component dioxygenase (Class IIB) comprising a flavoprotein (Red_{BED}) and a separate iron−sulfur protein (Fd_{BED}) for electron transfer to ISP_{BED}.

Several different classes of electron transfer proteins are known to bind [2Fe-2S] clusters [see Spiro (1982) and Cammack (1992)]. The most widespread arrangement of the clusters is typified by that found in plant and cyanobacterial ferredoxins, with two atoms of iron coordinated by bridging sulfurs and four cysteinyl sulfur atoms, as predicted from spectroscopic studies and confirmed by X-ray crystallography of *Spirulina platensis* ferredoxin (Fukuyama et al., 1980, 1995) and *Anabaena* ferredoxin (Rypniewski et al., 1991). Another class of [2Fe-2S] clusters is characterized by significantly different spectroscopic properties and more positive midpoint reduction potentials. The first of this type to be purified was isolated and characterized from the bc_1 complex of mitochondria by Rieske and co-workers (1964). Proteins with similar properties, present for example in the respiratory chain of the bacterium *Thermus thermophilus* (Fee et al., 1984) and from the b_6f complexes of the photosynthetic electron transfer chains (Malkin & Posner, 1978), are commonly referred to as "Rieske-type" proteins (Hatefi et al., 1962; Trumpower, 1981). This class of [2Fe-2S] clusters has E_m values (between +50 and +400 mV) which are considerably higher than those of plant-type ferredoxins ($E_m \sim -400$ mV), and their electron paramagnetic resonance (EPR) spectra are characterized by lower average g factors ($g_{av} \approx 1.91$, as compared with $g_{av} \approx 1.96$ for plant-type ferredoxins) and a more pronounced anisotropy (Bertrand et al., 1985). Another group of proteins, associated with certain types of oxygenases, has been proposed to belong to the Rieske class, on the basis of similarities in amino acid sequences and spectroscopic properties (Kuila et al., 1992; Mason & Cammack, 1992), despite having somewhat more negative midpoint potentials ($E_m \sim -150$ to -100 mV).

The amino acid sequence of ISP_{BED} contains the consensus sequence [$CxHx_{13-17}CxxH$], which is proposed to be the motif involved in binding all Rieske-type [2Fe-2S] centers (Mason & Cammack, 1992; Tan et al., 1993). However, although the EPR spectrum of the ISP_{BED} [2Fe-2S] cluster displays similarities to the spectra observed for Rieske-type proteins, some differences are nevertheless apparent. One such detail concerns the redox potential of ISP_{BED}, which is not as positive ($E_m = -115$ mV) (Geary et al., 1984) as the Rieske clusters of respiration and photosynthesis. Second, the EPR spectrum of ISP_{BED} is characterized by an even lower g_{av} value of 1.896 (g_x, g_y, g_z = 1.754, 1.917, and 2.018, respectively) (Crutcher & Geary, 1979). The causes of such differences in properties, which presumably have a functional significance, may be realized using spectroscopic approaches.

The EPR (Bertrand et al., 1985), electron nuclear double resonance (ENDOR) (Cline et al., 1985; Telser et al., 1987), Mössbauer (Fee et al., 1984), and resonance Raman (Kuila et al., 1987) spectra of the Rieske [2Fe-2S] centers in various proteins have been interpreted in terms of the presence of ligands more electronegative than sulfide at the Fe^{II} site. More recently, Gurbiel et al. (1989) made Q-band ENDOR measurements of a Class IA dioxygenase, *Pseudomonas cepacia* phthalate dioxygenase (PDO), using wild-type cells and histidine auxotrophs grown on [^{15}N]histidine and a ^{14}N background. In contrast to benzene dioxygenase (Class IIB), PDO comprises a flavin and iron−sulfur cluster combined in the same protein. These ENDOR studies established that two [^{15}N]histidine ligands are coordinated to the Rieske-type [2Fe-2S] cluster of PDO. Subsequently, the problem of which nitrogen (N^δ or N^ϵ) of the imidazole ring coordinates to the iron was addressed (Hoffman et al., 1993). ENDOR spectra of PDO uniformly labeled with ^{15}N and PDO labeled specifically with [$^{15}N^\delta$]histidine established that N^δ of the imidazole ring is directly coordinated to the iron. In the absence of a crystal structure of a protein containing a Rieske center, these studies have led to a structural model for Rieske-type centers in which two cysteine residues coordinate one Fe atom and both histidines coordinate to the Fe^{2+} site of the reduced cluster (Gurbiel et al., 1989, 1991; Hoffman, 1991). Site-directed mutagenesis studies of Rieske proteins have also suggested the essential requirement for cysteine and histidine residues (Graham & Trumpower, 1991; Davidson et al., 1992).

The pulsed EPR technique, electron spin-echo envelope modulation (ESEEM), is a convenient and discriminating method for observation of weak interactions of electron spins with nitrogen nuclei (Mims & Peisach, 1981). Fourier-transformed ESEEM spectra can provide information about the hyperfine coupling, and hence the strength of interaction of the paramagnetic center with the nucleus, and the quadrupole coupling, which gives an indication of the chemical form of the nitrogen. ESEEM of ferredoxin-type [2Fe-2S] clusters has detected only weakly coupled amide nitrogens (Orme-Johnson et al., 1983; Ackrell et al., 1984; LoBrutto et al., 1987; Cammack et al., 1988; Shergill & Cammack, 1994a; Dikanov et al., 1995), which are assigned to distant peptide nitrogens that are not directly coordinated to the cluster, on the basis of X-ray crystallographic studies on the *Spirulina* and *Anabaena* [2Fe-2S] ferredoxins (Fukuyama et al., 1980, 1995; Rypniewski et al., 1991). In contrast, the ESEEM spectra of the Rieske centers of spinach cytochrome b_6f complex and various bc_1 complexes (Telser et al., 1987; Britt et al., 1991; Shergill & Cammack, 1994b) displayed modulation frequencies corresponding to more strongly coupled nitrogens, in support of the ligand structure proposed by Gurbiel et al. (1989, 1991) for these centers. Using reasonable assumptions about the assignment of the ESEEM frequencies to distinct nitrogens (Britt et al., 1991), quadrupole couplings consistent with the imidazole nitrogens of histidine ligands were estimated.

ESEEM provides an additional means for comparison of the [2Fe-2S] clusters of oxygenases such as benzene dioxygenase with the Rieske proteins of respiration and photosynthesis. No major study of the ESEEM spectra of a

[1] Abbreviations: ISP_{BED}, benzene dioxygenase iron−sulfur protein; EPR, electron paramagnetic resonance; ENDOR, electron nuclear double resonance; ESEEM, electron spin-echo envelope modulation; FT, Fourier transform; HYSCORE, hyperfine sublevel correlation spectroscopy; NQI, nuclear quadrupole interaction; PDO, phthalate dioxygenase.

dioxygenase [2Fe-2S] cluster has been reported [see Shergill et al. (1994)]. Two-dimensional (2D) ESEEM spectra are an extension of the two- and three-pulse ESEEM methods, which allow the resolution of the complexity in spectra due to multiple hyperfine interactions (Höfer, 1991; Schweiger, 1991) but have had relatively few applications to metalloproteins. In the present study, we describe results on the ^{14}N coordination environment of the [2Fe-2S] cluster of *P. putida* ISP_{BED}, using 1D and 2D ESEEM spectroscopy. Herein, we have successfully employed the 2D ESEEM technique of hyperfine sublevel correlation spectroscopy (HYSCORE) to unambiguously correlate, for the first time, pairs of ESEEM frequencies belonging to certain hyperfine couplings, and hence different nitrogen nuclei. We have identified the presence of a third nitrogen, weakly coupled to the [2Fe-2S] cluster of ISP_{BED}. The results demonstrate the power of the 2D ESEEM techniques for resolving multiple hyperfine interactions.

EXPERIMENTAL PROCEDURES

P. putida strain ML2 was grown using benzene as the sole carbon source, as described by Geary et al. (1990). Cells were harvested in exponential growth phase, washed once with 25 mM potassium phosphate buffer (pH 7.2), and stored as a frozen paste at −20 °C. Cell extract was prepared essentially according to Geary et al. (1990) and treated with protamine sulfate in order to precipitate nucleic acids. The cell extract was then subjected to ammonium sulfate precipitation, (diethylamino)ethyl (DEAE) cellulose chromatography (Whatman DE52) and gel filtration (Sephacryl S-200). Further purification of ISP_{BED} was achieved by gel filtration chromatography with Ultrogel AcA 34 (LKB, Pharmacia). The purified protein was stored at −70 °C in 25 mM potassium phosphate (pH 7.2) containing 100 μM dithiothreitol. For ESEEM studies, protein samples of ISP_{BED} were concentrated by ultrafiltration through an Amicon PM10 membrane and reduced with a small excess of sodium dithionite under a stream of argon gas.

Pulsed EPR measurements were recorded at X-band on a Bruker ESP380 spectrometer, with a dielectric variable Q resonator (cavity quality factor, $Q \sim 100$; corresponding to a minimum dead time of ~100 ns) and an Oxford Instruments CF 935 liquid helium cryostat. ESEEM data were generally recorded at three magnetic field settings, corresponding to the principal g factors of the reduced ISP_{BED} [2Fe-2S] cluster. 1D ESEEM data were acquired with a three-pulse or stimulated-echo sequence ($\pi/2$-τ-$\pi/2$-T-$\pi/2$), using a phase-cycling routine, as described elsewhere (Shergill et al., 1991). The stimulated-echo amplitude was recorded as a function of T, whilst τ was kept constant. For the optimal detection of ^{14}N nuclei, the τ value (the time between microwave pulses I and II) was matched as closely as possible to a multiple of the proton Larmor frequency (ν_H), in order to suppress modulations due to weakly coupled protons (Mims & Peisach, 1981). Two types of 2D ESEEM spectra were recorded. In the first, the three-pulse sequence was used, and both τ and T were varied, giving a second dimension which was dependent upon the spin−spin relaxation time (T_2). Fourier transformation of the data in both dimensions (f_1 and f_2) resulted in the final 2D ESEEM spectra. The (f_1, f_2) data array was collected with intervals of 8 and 16 ns between each point, respectively. The 2D ESEEM HYSCORE data were collected using a four-pulse sequence ($\pi/2$-τ-$\pi/2$-T_1-π-T_2-$\pi/2$-echo) (Höfer, 1991). A spacing of 16 ns between each point was employed in both the f_1 and f_2 dimensions. The large number of unwanted two- and three-pulse echoes, which interfere with the echo from the four-pulse sequence, were removed by a four-step phase-cycling routine (Gemperle et al., 1990). The ESEEM data collected were Fourier transformed using the Bruker pulsed spectra manipulation routines (ESP 380 software for 1D ESEEM; WinEPR software for 2D ESEEM data).

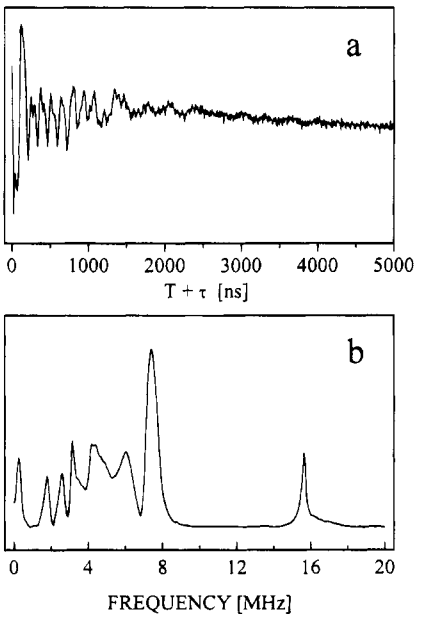

FIGURE 1: Three-pulse ESEEM spectra of *P. putida* ISP_{BED}, recorded at $g_y = 1.914$: (a) echo decay envelope and (b) Fourier transform. Measurement conditions were as follows: temperature, 3.8 K; τ value, 112 ns; pulse width (for a 90° pulse), 16 ns; band width, 100 MHz; microwave frequency, 9.77 GHz; B_0, 365.1 mT; number of shots, 8; video amplifier gain, 42 dB; traveling wave tube attenuation, 8 dB; and shot repetition time, 10.24 ms.

RESULTS

1D ESEEM Spectroscopy of ISP_{BED}. Figure 1 displays the three-pulse ESEEM spectrum of the *P. putida* ISP_{BED} [2Fe-2S] cluster, recorded using a τ value of 112 ns at $g_y = 1.91$. The frequency spectrum (Figure 1b), obtained by Fourier transformation of the time domain data presented in Figure 1a, shows clearly resolved features at *ca.* 1.8, 2.6, 3.5, 4.5, 6.1, 7.5, and 15.5 MHz. The 15.5 MHz modulation corresponds to the incompletely suppressed ^1H nuclear Zeeman frequency and is assigned to the remote proton nuclei in the protein and/or water environment. The frequencies in the 1−10 MHz region are attributed to ^{14}N couplings. They extend to higher values than those observed for ^{14}N couplings to the ferredoxin class of [2Fe-2S] clusters. The crystal structure of *S. platensis* and *Anabaena* ferredoxins shows that the [2Fe-2S] center is coordinated by four cysteinyl sulfur atoms and interacts with distant peptide nitrogens (Fukuyama et al., 1980, 1995; Rypniewski et al., 1991); the maximum frequency observed with *S. platensis* ferredoxin is *ca.* 4.5 MHz (Ackrell et al., 1984; Cammack et al., 1988; Shergill et al., 1991; Shergill & Cammack, 1994a; Dikanov et al., 1995). Instead, the frequencies detected are consistent with a stronger superhyperfine interaction between the [2Fe-2S] cluster of ISP_{BED} and ^{14}N nuclei.

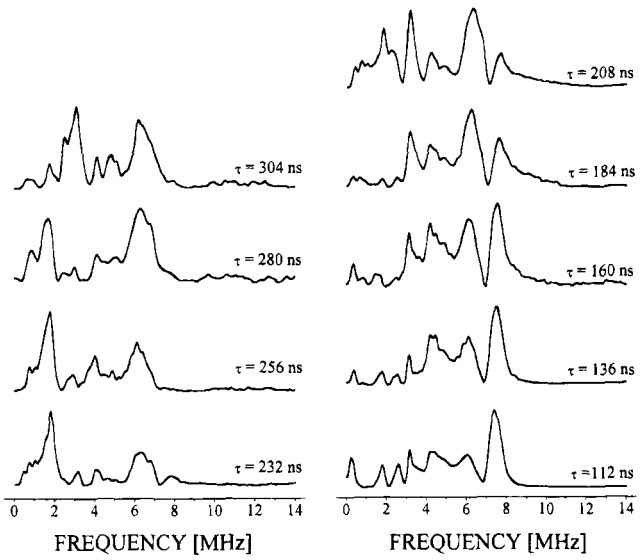

FIGURE 2: Fourier transforms of the three-pulse ESEEM spectra of *P. putida* ISP_{BED}, recorded at $g_y = 1.914$. The values of τ employed are indicated in the figure. Other measurement conditions were as described for Figure 1.

As the amplitudes of electron spin-echo modulations are a periodic function of τ (Mims, 1972a,b), certain frequencies of interest may be suppressed at any one τ value. By comparing ESEEM spectra recorded at the same field position but with different τ values, we have probed the anisotropic broadening of the features due to ^{14}N nuclei. Figure 2 demonstrates that the position and, in particular, the intensity of these low-frequency components varied as a function of τ, with the highest frequency component at ~7.5 MHz detected most clearly at low values of τ. The other high-frequency component at ~6 MHz was more prominent at higher values of τ. In all, as many as nine features were resolved in the 0−10 MHz region of the spectra. There can be no more than six distinct modulations associated with a single ^{14}N nucleus; of these, no more than four have been observed to give rise to resolved lines in frozen solution samples (Mims & Peisach, 1978). We therefore propose that the spectra presented in Figure 2 arise from an interaction of the ISP_{BED} [2Fe-2S] cluster with more than one ^{14}N nucleus.

The ESEEM pattern of ISP_{BED} may be provisionally assigned by comparison with the ESEEM spectra of Rieske [2Fe-2S] clusters. For example, similar modulation frequencies have been observed with the Rieske proteins of respiration and photosynthesis (Britt et al., 1991; Shergill & Cammack, 1994b). Partly on the basis of these Rieske proteins displaying two peaks characteristic of the so-called double quantum (ν_{dq}^+) transitions in the 5−8 MHz region, the ^{14}N modulations observed were assigned by these authors as due to two nitrogen ligands. The spectra presented in Figures 1 and 2, as with all previously published ESEEM studies of Rieske centers, were acquired at a magnetic field near to g_y, in order to obtain maximum spin-echo intensity. However, the ESEEM patterns obtained at this position do not arise from a single orientation but instead represent the sum of spectra arising from a range of orientations of the molecule with respect to the static field (Hoffman et al., 1984). There is thus a potential ambiguity of interpretation; the presence of two lines might, for example, represent either two different nuclei, giving different hyperfine couplings, or one nucleus with an anisotropic hyperfine coupling, observed in two different orientations. Data collected at multiple magnetic fields are required to fully characterize nuclei coupled to paramagnetic centers with rhombic **g** tensors.

Figure 3 displays the orientation selection spectra obtained at g_z and g_x. These spectra are less intense than those recorded at g_y, but each represents a unique orientation of the ISP_{BED} [2Fe-2S] cluster with respect to the field, giving a "single-crystal-like" pattern (Rist & Hyde, 1970). The FT spectrum obtained at $g_z = 2.02$ displayed an intense feature centred at *ca.* 3.2 MHz and two less intense features at *ca.* 4.5 and 7.2 MHz (Figure 3a). An increase of magnetic field to $g = 2.00$ resulted in the splitting of the 3.2 MHz feature into two intense peaks centered at *ca.* 3.2 and 3.5 MHz (data not shown). Only one feature (7.2 MHz) characteristic of a ν_{dq}^+ transition resulting from an interaction between a ^{14}N nucleus and a Rieske center (Britt et al., 1991) was observed at these g factors, despite varying τ. By increasing the field further to $g \sim 1.95$, we observed features characteristic of two ν_{dq}^+ transitions in the 5−8 MHz region (data not shown). This spectrum is essentially identical to that obtained at $g_y = 1.91$ (see Figure 1b), differing slightly in the relative position and amplitude of lines which are expected to vary as a function of g_{eff}, corresponding to the relative orientation of the hyperfine and quadrupolar coupling tensors with respect to the **g** matrix (Mims, 1972). The spectrum recorded at the single-crystal-like position $g_x = 1.76$ (Figure 3b) also displayed two weak features at ~6.2 and 7.7 MHz. This observation confirms that the two highest frequency ^{14}N resonances are indeed due to two different nitrogen nuclei. Changes were also observed in the features in the 2−3.6 MHz and the 5−8 MHz regions, which shifted toward high frequency with increasing field.

Interpretation of the ^{14}N Modulation Frequencies of ISP_{BED}. The ESEEM technique applied here allows the calculation of parameters related to the energies of nuclear spin states of any ^{14}N nuclei. The interactions giving rise to the ESEEM effect include the electron−nuclear hyperfine interaction (A), which provides information on the extent of unpaired electron spin density on the nucleus, and the nuclear quadrupolar interaction (NQI), which reflects the bonding interactions of that atom. The NQI is described by a coupling constant (e^2qQ), which indicates the magnitude of the electric field gradient, and an asymmetry parameter (η), which describes charge asymmetry. If the hyperfine coupling results in "exact cancellation" ($A \approx 2\nu_N$, *ca.* 2.25 MHz at 365.1 mT) (Mims & Peisach, 1978; Flanagan & Singel, 1987), the ESEEM spectrum comprises three sharp lines and a broader fourth line (Lucken, 1969; Mims & Peisach, 1989). This pattern is however not apparent in the ESEEM spectra of ISP_{BED} (see Figures 1−3), indicating that the modulation is due to ^{14}N hyperfine values of >2.25 MHz (*i.e.*, $A > 2\nu_N$). In the latter case, four of the lines are broadened while two remain sharp. The latter arise from the double quantum ($\Delta M_I = 2$) transitions, ν_{dq}^- and ν_{dq}^+, one from each electron spin manifold (Flanagan & Singel, 1987; Britt et al., 1991; Dikanov & Tsvetkov, 1992). Consequently, in order to assign the ISP_{BED} ESEEM frequencies, we have applied the theoretical analyses of Dikanov and Tsvetkov (1992) (eq 1):

$$\nu_{dq}^{\pm} = 2[(\nu_N \pm |A/2|)^2 + (e^2qQ/4)^2(3 + \eta^2)]^{1/2} \quad (1)$$

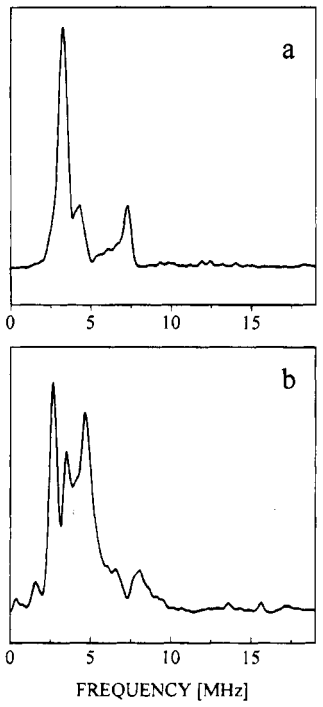

FIGURE 3: Three-pulse ESEEM Fourier transform spectra showing the "single-crystal-like" patterns obtained with *P. putida* ISP_{BED} at (a) g_z and (b) g_x. Measurement conditions were as described for Figure 1, except as follows: τ value, (a) 136 and (b) 120 ns; B_0, (a) 344.9 and (b) 396.0 mT; number of shots, (a) 10 and (b) 30; video amplifier gain, 57 dB; traveling wave tube attenuation, (a) 8 and (b) 6 dB.

where ν_N is the ^{14}N nuclear Zeeman frequency. From this equation, the values of the ^{14}N hyperfine and quadrupolar couplings may be estimated; the value of η gives rise to a relatively minor uncertainty. In the present case, η values in the range 0.25−0.69 resulted in differences of less than ±10% in our estimates of e^2qQ.

The similarities in the ESEEM spectra of ISP_{BED} and Rieske protein [2Fe-2S] centers (Britt et al., 1991; Shergill & Cammack, 1994b) indicate that the dioxygenase data represent the superimposition of signals from two ^{14}N nuclei. For these nuclei, two pairs of $\Delta M_I = \pm 2$ frequencies (*i.e.* two ν_{dq}^- and two ν_{dq}^+ peaks) are expected, and these have to be assigned to each nitrogen in order to estimate the superhyperfine coupling parameters, on the basis of reasonable assumptions about the magnitudes of the expected quadrupole couplings. In the spectrum of ISP_{BED} recorded at g_y, six main lines were observed at *ca.* 1.8, 2.6, 3.5, 4.5, 6.1, and 7.5 MHz (Figure 1b). Following Britt et al. (1991), we assign the 2.6, 3.5, 6.1, and 7.5 MHz frequencies to $\Delta M_I = \pm 2$ transitions. Of the two possible pairing combinations, the (2.6, 7.5) and (3.5, 6.1) pairing arrangement gives $e^2qQ \approx 3.85$ MHz for N(1) and $e^2qQ \approx 0$ MHz for N(2). A zero value for the electric field gradient is unlikely for a ^{14}N nucleus in a protein environment (Edmonds & Speight, 1971; Ashby et al., 1978). The alternative pairing of (2.6, 6.1) and (3.5, 7.5) yields reasonable values for the ^{14}N coupling parameters: $A_y = 3.33$ MHz and $e^2qQ = 2.62 \pm 0.1$ MHz for N(1) and $A_y = 4.79$ MHz and $e^2qQ = 2.69 \pm 0.1$ MHz for N(2) (Table 1).

Pairings of these modulation frequencies with the prominent features at ~1.8 and ~4.5 MHz (see Figure 1b) give rise to unlikely values of e^2qQ, when compared with the values reported for ^{14}N of either a peptide or imidazole group

Table 1: Hyperfine and Quadrupolar Coupling Constants for the Nitrogens Coupled to the [2Fe-2S] Cluster of *P. putida* ISP_{BED}[a]

	ISP_{BED} principal values (MHz)		
	N(1)	N(2)	N(3)
	Hyperfine Coupling		
A_z	3.36 ± 0.12 (6)	4.44 ± 0.19 (6)	
A_y	3.50 ± 0.14 (4)	4.99 ± 0.16 (4)	1.11 ± 0.04 (2)
A_x	3.82 ± 0.13 (3)	4.92 ± 0.12 (3)	
A_{iso}[b]	3.56	4.78	
	Quadrupolar Coupling[c]		
$e^2qQ_{(g_z)}$	2.17 ± 0.07	2.17 ± 0.07	
$e^2qQ_{(g_y)}$	2.46 ± 0.08	2.33 ± 0.07	3.27 ± 0.01 (2)
$e^2qQ_{(g_x)}$	2.78 ± 0.09	2.38 ± 0.08	

[a] The coupling constants represent the mean ± standard deviation, with the number of data sets in parentheses. The subscripts x, y, and z refer to the principal axes of the **g** matrix. [b] $A_{iso} = {}^1/_3(A_x + A_y + A_z)$. e^2qQ was estimated from the ESEEM spectra recorded at g_z, g_y, and g_x, respectively, using a value of $\eta = 0.5$ for N(3) and by varying η between 0.25 and 0.69 for N(1) and N(2).

(Edmonds & Speight, 1971; Ashby et al., 1978; Gurbiel et al., 1989, 1991; Britt et al., 1991; Shergill & Cammack, 1994b). We have therefore looked for other explanations for these two features. They could be due to either the single quantum ($\Delta M_I = 1$) transitions of the two ^{14}N nuclei, combination lines as a result of multiple ^{14}N nuclei, or perhaps a third nitrogen. Their assignment will be discussed later.

2D ESEEM Spectroscopy of ISP_{BED}. Three-pulse 2D ESEEM experiments are expected to provide greater spectral resolution of nuclear modulation due to the second spectral dimension. Contributions from the two, or perhaps more, ^{14}N nuclei coupled to the ISP_{BED} [2Fe-2S] cluster may be unravelled by the 2D technique which correlates those modulation frequencies sharing the same hyperfine coupling (Höfer, 1991). Firstly, if the value of τ is varied in one dimension, the possibility of blind spots is eliminated. Secondly, the ambiguities in the assumed pairing arrangements of the double quantum features can be resolved. The 2D ESEEM data sets measured at the three g values of the [2Fe-2S] cluster (Figure 4) were obtained by performance of the stimulated-echo experiment over a range of τ values, using $\pi/2$ microwave pulses. This gives a 2D spectrum with T as one variable and τ as the other. The spectra shown in Figure 4a−c were Fourier transformed in the f_2 dimension only and therefore represent τ-swept frequency domain spectra at g_z, g_y, and near g_x.

The FT spectra from the 2D ESEEM pattern acquired at g_z are shown in Figure 4a and clearly illustrate the presence of frequencies due to ^{14}N nuclei in the 0−8 MHz region. Although a similar spectrum was obtained with the 1D technique at the same g-value we failed to resolve the two ν_{dq}^+ features characteristic of two ^{14}N nuclei expected in the 5−8 MHz region (see Figure 3a). However, in the 2D pattern recorded at g_z, the slices corresponding to high values of τ (400−424 ns) display distinct peaks in the 0−5 MHz region and also two high-frequency peaks in the 5−8 MHz region (see Figure 4a inset). These high-frequency $\Delta M_I = 2$ features are intense and clearly resolved. Each slice along the f_2 dimension of the $g_y = 1.91$ 2D ESEEM spectra gave essentially the same information as the individual 1D spectra acquired at various τ values (*cf.* Figures 2 and 4b). Two ν_{dq}^+ features were also clearly observed in the 5−8 MHz region of the 2D ESEEM FT spectra acquired at the single-

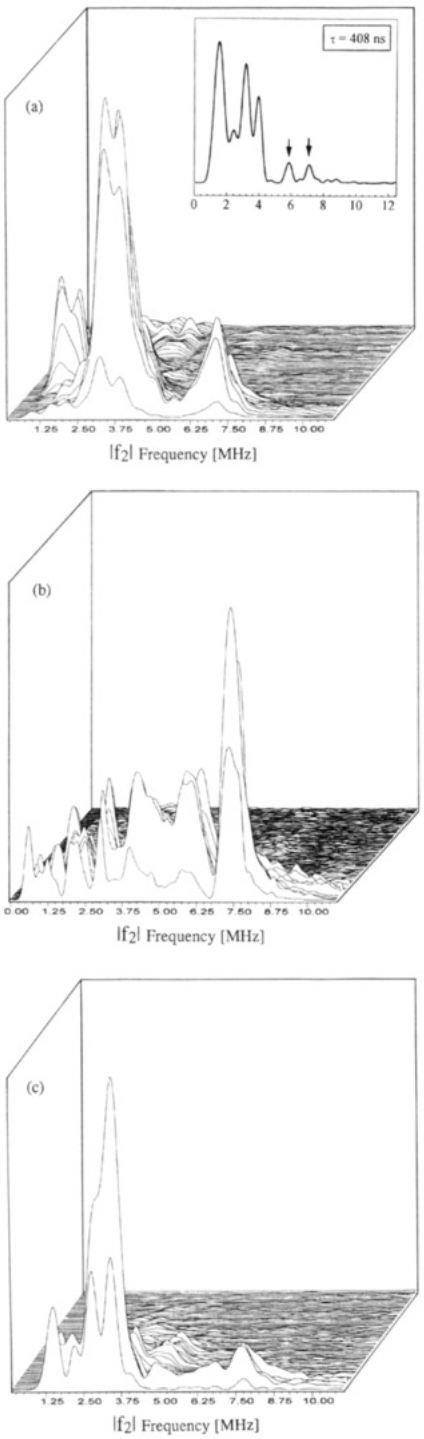

FIGURE 4: 2D ESEEM FT spectra of *P. putida* ISP_{BED}, recorded at (a) $g_z = 2.02$, (b) $g_y = 1.914$, and (c) $g \sim 1.80$. The spectra presented were obtained by Fourier transformation of data in $|f_2|$ only. The inset, showing a single slice of the g_z 2D ESEEM pattern corresponding to a τ value of 408 ns demonstrates the presence of two well-resolved double quantum features in the 5−8 MHz region (see text for details). Measurement conditions were as follows: microwave frequency, (a and c) 9.78 and (b) 9.77 GHz; B_0, (a) 345.0, (b) 365.1, and (c) 387.1 mT; spectral resolution of $|f_1|$, 256; spectral resolution of $|f_2|$, (a) 64 and (b and c) 128; stepsize $|f_1|$, (a) 8 and (b and c) 16 ns; stepsize $|f_2|$, (a and c) 8 and (b) 16 ns; number of shots, (a) 8 and (b and c) 4; band width, 100 MHz; shot repetition time, 10.24 ms; sample temperature, 3.8 K.

crystal-like field setting near g_x, at *ca.* 6.6 and 7.6 MHz, in addition to the two υ_{dq}^- features, at *ca.* 2.6 and 3.4 MHz (Figure 4c). Observation of features assignable to *two* $\upsilon_{dq}^{\pm}$ transitions in the 2D ESEEM spectra, at both g_{min} and g_{max},

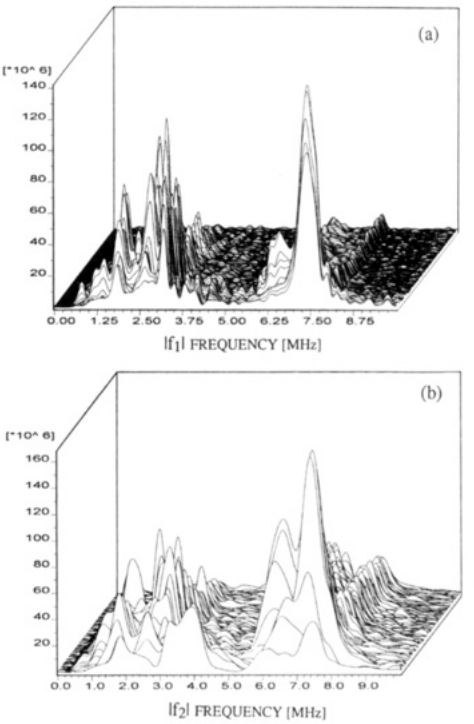

FIGURE 5: HYSCORE FT spectra of *P. putida* ISP_{BED}, recorded at $g_y = 1.914$. Data were Fourier transformed in either the (a) $|f_1|$ or (b) $|f_2|$ dimensions only. Measurement conditions were as follows: microwave frequency, 9.81 GHz; B_0, 365.9 mT; spectral resolution of $|f_1, f_2|$, 256; stepsize $|f_1, f_2|$, 16 ns; number of shots, 8; band width, 100 MHz; shot repetition time, 10.24 ms; high-power pulse attenuation, 8 dB; video amplifier gain, 45 dB; sample temperature, 3.8 K.

further verifies that the ESEEM spectra obtained with the [2Fe-2S] cluster of ISP_{BED} result from an overlap of at least two nitrogens.

HYSCORE Spectroscopy of ISP_{BED}. The HYSCORE experiment, which utilizes a four-pulse sequence (Höfer, 1991), is derived from the three-pulse 2D ESEEM experiment and includes a π pulse to exchange the populations of the electron energy m_s levels, creating correlations between nuclear spin transitions associated with the two electron spin levels. One advantage of this method is that the decay of the modulations is a function of the spin−lattice relaxation rate only, as opposed to both spin−lattice and spin−spin relaxation rates, giving enhanced spectral resolution (Höfer, 1991).

The HYSCORE FT spectra of ISP_{BED}, recorded at $g_y = 1.91$, are presented in Figure 5. The data were Fourier transformed in either the f_1 or the f_2 dimension. The four features corresponding to the two $\upsilon_{dq}^{\pm}$ transitions of the two strongly coupled nitrogens are clearly observed in the HYSCORE spectrum, in both dimensions. The major peak previously observed at ~4.5 MHz in the g_y 1D and 2D ESEEM spectra is however not a dominating feature of the HYSCORE spectrum (*cf.* Figure 5 with Figures 1b and 4b). This is probably due to the suppression effect encountered in the HYSCORE experiment; the blind spots in the modulation pattern are induced as a result of the fixed waiting time τ, upon which the 2D FT pattern is dependent (Höfer, 1991; Shane et al., 1992).

The same HYSCORE data are presented as a contour plot in Figure 6, after Fourier transformation of both f_1 and f_2 dimensions. Features which are hyperfine-coupled, for

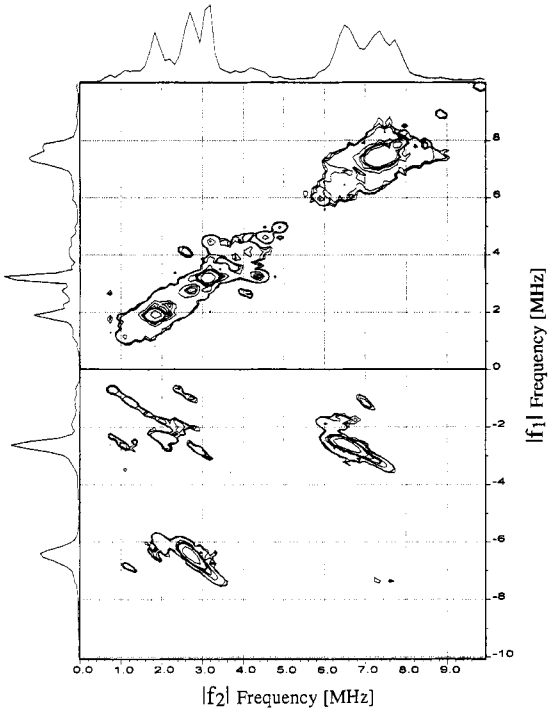

FIGURE 6: Contour plot representation of the $g_y = 1.914$ HYSCORE spectrum recorded for *P. putida* ISP_{BED}.

Table 2: Cross-Peaks (*P* and *P'*) Observed in the $[-f_1, +f_2]$ Quadrant of the HYSCORE Contour Plot Recorded at $g_y = 1.914$ for *P. putida* ISP_{BED}

	$\nu_{observed}$ (MHz)	
	P	*P'*
1	−2.5, +1.1	−1.0, +2.6
2	−3.6, +1.0	−1.0, +3.8
3	−6.3, +1.8	−1.8, +6.3
4	−6.4, +2.7	−2.6, +6.5
5	−6.9, +1.1	−1.0, +6.9
6	−7.3, +3.3	−3.2, +7.2

example the peaks corresponding to the (3.5, 7.5; $A_y \sim 4.99$ MHz) pair observed in the 1D ESEEM spectra (Figure 1b), are labeled by off-diagonal peaks (cross-peaks) in the 2D spectrum; these are prominent in the negative f_1 region ($[+f_2, -f_1]$quadrant) of the plot. At least six pairs of cross-peaks are observed in the contour plot, positions of which are summarized in Table 2. The two pairs of cross-peaks in the [+, −] quadrant at *ca.* [(2.7, −6.4), (6.5, −2.6)] and [(3.3, −7.3), (7.2, −3.3)] MHz, correspond to the $\nu_{dq}^{\pm}$ frequencies of the two ^{14}N nuclei proposed to coordinate the [2Fe-2S] cluster of ISP_{BED}. As these cross-peaks correlate the pairs of ESEEM lines belonging to certain hyperfine couplings (*i.e.* $A_{iso} \sim 3.56$ and 4.78 MHz, respectively), the contour plot confirms the assignment of lines in the 1D spectra to the $\Delta M_I = 2$ transitions of two distinct nitrogens, and thus the estimates of hyperfine and quadrupolar coupling constants for the ^{14}N nuclei.

It is interesting to note that the diagonal, which is due to an incomplete inversion by the π pulse (Gemperle et al., 1990; Höfer, 1991), is confined to the positive f_1 region ([+, +] quadrant) (Figure 6). As the $|+f_1|$ and the $|-f_1|$ regions are defined by $A < 2\nu_N$ and $A > 2\nu_N$ (where $2\nu_N \sim 2.25$ MHz for ^{14}N nuclei at $B_0 = 365.1$ mT), respectively, the confinement of the cross-peaks to the [+, −] quadrant also verifies the A_{iso} values determined for the two nitrogens, 3.56 and 4.78 MHz for N(1) and N(2), respectively. Furthermore,

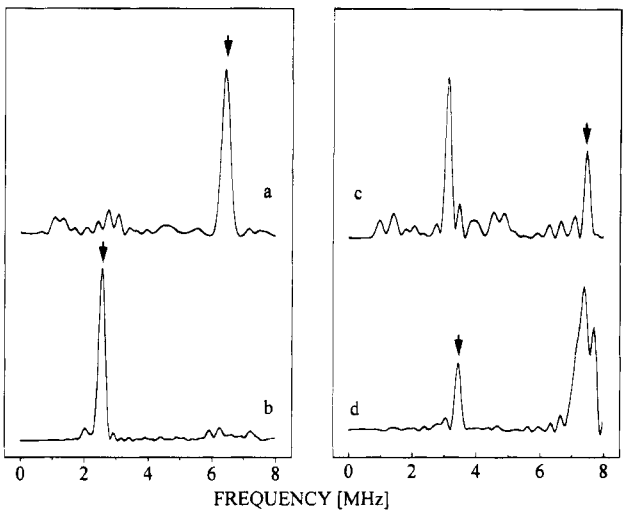

FIGURE 7: FT spectra of individual HYSCORE $|f_1|$ slices, obtained at frequencies corresponding to the $\Delta M_I = 2$ transitions of N(1) at *ca.* (a) 2.6 and (b) 6.2 MHz and N(2) at *ca.* (c) 3.5 and (d) 7.5 MHz. Measurement conditions were as for Figure 5.

it is evident from Figure 6 that the cross-peaks are narrow and parallel to the diagonal. This can be explained by a relatively small anisotropic hyperfine interaction, which is also responsible for the line shape of the double quantum transitions in the 1D spectra. Also, when two transitions have a similar orientation dependence, a correlation ridge along the diagonal is expected, as opposed to perpendicular to the diagonal when the two transitions have an opposite orientation dependence (Shane et al., 1992). Consequently, we can infer a one-to-one relationship between the ν_{dq}^- and ν_{dq}^+ line shapes at any given orientation of the magnetic field.

Correlation of Transitions Using Individual f_1 Slices from the HYSCORE Spectrum. When the HYSCORE spectrum of ISP_{BED} in the f_2 dimension only was Fourier transformed, a τ-swept 1D ESEEM spectrum consisting of 256 slices was obtained. The time domain data in the f_1 dimension comprise 256 slices, each of which correlates with a particular nuclear frequency. Fourier transformation of the f_1 slice corresponding to a nuclear frequency of 2.6 MHz gave a spectrum comprising one dominating peak at ~6.4 MHz (Figure 7a), while the FT subspectrum corresponding to 6.2 MHz comprised a peak at ~2.5 MHz (Figure 7b). Similarly, the FT subspectrum corresponding to ~3.5 MHz contained two peaks at *ca.* 3.15 and 7.45 MHz, with minor peaks in the 1−7 MHz region (Figure 7c), while the FT subspectrum corresponding to ~7.5 MHz consisted of two major peaks at ~3.4 and ~7.5 MHz (Figure 7d). Since cross-correlations are expected for transition pairs (ν_{dq}^- and ν_{dq}^+), this procedure eliminates any remaining uncertainty over the assignment of the pairs of transitions at *ca.* (2.6, 6.1) and (3.5, 7.5) MHz to individual ^{14}N hyperfine couplings. N(1) and N(2) are identified as the ligands to the [2Fe-2S] cluster of ISP_{BED}, as seen in the ENDOR spectra of PDO.

Assignment of the 1.8 and 4.5 MHz Features. Additional intense resonances at 1.8 and 4.5 MHz were observed in the 1D and 2D FT ESEEM spectra of ISP_{BED} recorded at g_y (Figures 1b, 2, and 4b). Similar resonances at 1−2 and 4−5 MHz were also observed in the spectra recorded at g_z and g_x (Figures 3 and 4a,c). We note that similar features are present in the published ESEEM spectra of the *Thermus*

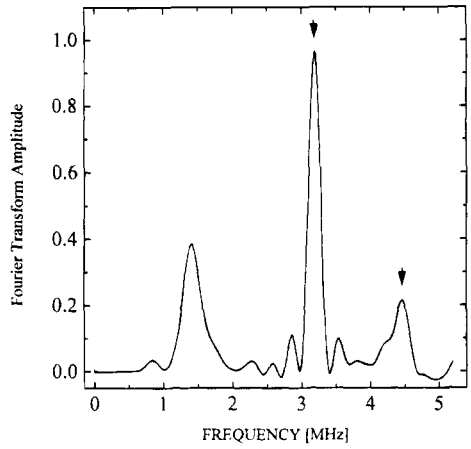

FIGURE 8: FT spectrum of an $|f_1|$ slice from the ISP_{BED} HYSCORE spectrum. The chosen slice correlated with a nuclear frequency of 4.53 MHz (see text). Measurement conditions were as for Figure 5.

Rieske protein (Cline et al., 1985), and there is significant intensity in the same regions in the three-pulse ESEEM spectra of the Rieske centers of the spinach cytochrome b_6f complex and *Rhodospirullum rubrum*, *Rhodobacter sphaeroides* R-26, and bovine heart bc_1 complexes (Britt et al., 1991; Shergill & Cammack, 1994b). These additional resonances were not correlated with the transitions corresponding to the two strongly coupled nitrogens, N(1) and N(2).

In order to identify other frequencies with which the 1.8 MHz feature may correlate, we have analyzed f_1 slices of the g_y HYSCORE spectrum corresponding to this nuclear frequency. The FT subspectra of f_1 slices synonymous with 1.71 and 1.83 MHz essentially showed only one major feature at ~1.8 MHz, preventing any cross-correlation with other features in the 0−10 MHz region (data not shown).

The FT subspectra of f_1 slices corresponding to 4.41 and 4.53 MHz each displayed three intense features at *ca.* 1.4, 3.2, and 4.5 MHz (Figure 8), which we attribute to a hyperfine interaction with a third nitrogen. The coupling parameters for this nitrogen may be estimated using the theoretical analyses of Dikanov and Tsvetkov (1992), by assignment of the two highest frequencies to a ^{14}N $\Delta M_I = 2$ transition ($\nu_{dq}^{\pm}$). Assuming a value of $\eta = 0.5$, couplings of $A_y = 1.11 \pm 0.04$ MHz and $e^2qQ = 3.27 \pm 0.01$ MHz are estimated. These coupling parameters are almost identical to the values determined for other iron−sulfur proteins containing ferredoxin-type [2Fe-2S] clusters which interact weakly with peptide nitrogen (Cammack et al., 1988; Shergill & Cammack, 1994a; Dikanov et al., 1995). The possibility of an interaction between the [2Fe-2S] cluster of ISP_{BED} and a third noncoordinating nitrogen of the polypeptide chain therefore exists.

DISCUSSION

The coupling parameters derived for the three nitrogens coupled to the ISP_{BED} [2Fe-2S] cluster are summarized in Table 1. The quadrupolar coupling e^2qQ depends on the electric field gradient at the nucleus and is characteristic of the type of nitrogen giving rise to the ESEEM effect. The estimates of e^2qQ for N(1) and N(2) fall within the range of values reported for the imino nitrogen of imidazole coordinated to metal ions ($e^2qQ = 1.93-2.82$ MHz, for $\eta = 0.69-0.25$) (Ashby et al., 1978). These values are comparable with those of the histidine ligands identified in *P. cepacia* PDO (2.6 and 2.3 MHz) by ENDOR and specific isotope substitution (Gurbiel et al., 1989, 1991). Similar e^2qQ values were reported for spinach cytochrome b_6f complex (2.5−2.9 MHz for both ^{14}N nuclei) (Britt et al., 1991) and bovine heart cytochrome bc_1 complex (2.25 ± 0.15 and 2.93 ± 0.23 MHz) (Shergill & Cammack, 1994b). The values for the third nitrogen, (N3), are within the range of values reported for peptide ^{14}N in di- and tripeptide compounds (e^2qQ = 3.0−3.4 MHz, for $\eta = 0.4-0.5$) (Edmonds & Speight, 1971; Hunt & Mackay, 1976).

The isotropic hyperfine coupling parameters ($A_{iso} = 3.56$ and 4.78 MHz) for nitrogens N(1) and N(2) are consistent with direct ligation to the iron of the [2Fe-2S] cluster of ISP_{BED}. Since the couplings are similar in magnitude, they are assigned to the proximal nitrogens of two different imidazole ligands, as opposed to the bonding and nonbonding nitrogens of the same histidine residue. In the latter case, the couplings are expected to differ by a factor of ≥20, as demonstrated for Cu^{2+}−imidazole complexes (van Camp et al., 1981). The A_{iso} values for N(1) and N(2) are generally in good agreement with those obtained for the two [^{15}N]-histidine ligands of the Rieske-type centers by simulation of the ENDOR spectra of *P. cepacia* PDO [$A_{iso}^{(14N)} = 4.3$ and 5.5 MHz] and *R. capsulatus* bc_1 complex [$A_{iso}^{(14N)} = 4.5$ and 5.5 MHz] (Gurbiel et al., 1989, 1991). The differences in A_{iso} between the ESEEM-derived ISP_{BED} data and the ENDOR-derived data may reflect the different spectroscopic techniques employed. A closer match is observed upon comparison of our results with the ESEEM studies of Rieske centers, for example, the work of Britt et al. (1991) on the b_6f complex ($A_y \sim 3.8$ and 4.6 MHz) and Shergill and Cammack (1994b) on the bovine heart bc_1 complex ($A_y \sim 3.6$ and 5.2 MHz).

The amino acid sequence of ISP_{BED} contains the consensus sequence [$C^{96}xH^{98}x_{13-17}C^{116}xxH^{119}$] which is proposed to bind Rieske-type centers. It seems clear that the two ^{14}N ligands to the [2Fe-2S] cluster are derived from His^{98} and His^{119}, as confirmed by site-directed mutagenesis studies (Butler, 1995). The unpaired electron is unequally delocalized on the two histidines, with greater electron density at N(2), making the coordination at this site more covalent. In the absence of a crystal structure, the answer to the question of whether N(2) represents His^{98} or His^{119} must await our current studies on the altered environment of the [2Fe-2S] cluster in site-directed mutants of *P. putida* ISP_{BED}. As a difference in A_{iso} between N(1) and N(2) is observed for all Rieske-type centers investigated thus far ($\Delta A_{iso} = 0.8-1.6$ MHz), it is unlikely that ΔA_{iso} accounts for the differences in the redox potentials of the Rieske-type proteins of aromatic dioxygenases and respiratory chains, with the former exhibiting less positive values of E_m than the latter. The range in the magnitude of ΔA_{iso} for the various Rieske-type centers may reflect a difference in geometry at the Fe^{2+} site, which could be due to either structural differences and/or a rearrangement of orbital directions (Jiang et al., 1991).

The hyperfine couplings for N(1) and N(2) are fairly isotropic (see Table 1). It appears that the anisotropy in A estimated for N(2) gives an axial form ($A_y = A_x$), with the smallest value ($|A_z|$) occurring for the hyperfine principal axis component aligned near g_z. For example, the highest frequency component in the ESEEM spectra (1D and 2D) recorded at $g_z = 2.02$ occurs at ~7.2 MHz but occurs at

Table 3: Bonding Parameters Estimated for the Two ^{14}N Nuclei Coordinating the [2Fe-2S] Center of *P. putida* ISP_{BED}

	f_{2s} (%)			f_{2p} (%)		a_{2p}		a_{3d}	
nitrogen	ISP_{BED}[a]	PDO[b]	bc_1[c]	ISP_{BED}	PDO	ISP_{BED}	PDO	ISP_{BED}	PDO
N(1)	1.29	~1.5	~1.7	0.2	≥1	0.03	~0.2	~0.6	~0.75
N(2)	1.73	~2	~2	1.4	≥1	0.24	~0.2	~0.6	~0.75

[a] This work. [b] Gurbiel et al. (1989). [c] Gurbiel et al. (1991).

~7.7 MHz in the spectra recorded at $g_x = 1.76$ (Figures 3 and 4). The anisotropic component can have contributions from spin density in the 2p orbital on nitrogen as well as from direct dipolar interaction with the Fe^{2+} ion of the cluster. The possibility of the coupling arising entirely from a through-space dipolar interaction without covalent Fe−N bonding can be eliminated, as this would give $A_z = A_y = -A_x/2$ (Atherton, 1973; Gurbiel et al., 1989). Therefore, the two nitrogens coupled to the [2Fe-2S] center of *P. putida* ISP_{BED} have a considerable isotropic component arising from electron spin density in the ^{14}N 2s valence orbital, which strongly suggests that the cluster is covalently bonded by two ^{14}N nuclei.

Estimation of ^{14}N Ligand Bonding Parameters. The hyperfine couplings of N(1) and N(2) reported in Table 1 are defined in terms of the nuclear spin interaction with the total electron spin of the spin-coupled [2Fe-2S] cluster of ISP_{BED}. However, the ^{14}N couplings arise from a nuclear hyperfine interaction with the isolated local spin on that site (Fe^{3+}, $S = 5/2$; Fe^{2+}, $S = 2$) having a coupling constant $\mathbf{a}(i)$, $i = 1$ or 2. Using the spin-coupling model of Gibson et al. (1966) ($\mathbf{a}_{(i)} = -3/4\ \mathbf{A}_{(i)}$), the fundamental hyperfine tensor $\mathbf{a}(i)$ describing the ^{14}N interaction with the spin of the Fe^{2+} site can be related to the measured hyperfine tensor $\mathbf{A}(i)$ describing the electron-nuclear interaction with the [Fe^{2+}:Fe^{3+}] spin-coupled $S = 1/2$ pair (Gurbiel et al., 1989). The following interpretation of the hyperfine couplings to determine the fraction of unpaired Fe^{2+} electron spin (f_{2s}) residing in the 2s orbital of N(1) and N(2) is based upon the analyses employed by Gurbiel et al. (1989, 1991) for Rieske-type centers. ^{15}N values of A_{iso} were obtained for ISP_{BED} by multiplying the ^{14}N values by 1.403 [$^{15}N(1) = 5.0$ MHz and $^{15}N(2) = 6.7$ MHz], in order to directly compare the electron spin density distribution with the analyses of Gurbiel et al. (1989) for ^{15}N-enriched PDO.

By relating f_{2s} to a_{iso}, we have estimated values of $f_{2s}(N1) = 1.29\%$ and $f_{2s}(N2) = 1.73\%$ for the Fe^{2+} site of the ISP_{BED} [2Fe-2S] cluster. Similarly, we have estimated the anisotropic component of the hyperfine coupling, which has a local contribution (a_{2p}) arising from direct dipolar coupling to the Fe^{2+} ion (a_{3d}), and from unpaired density in the 2p orbital on nitrogen (f_{2p}). These values are summarized in Table 3. For a simple sp^2 orbital scheme, Scholes et al. (1982) have predicted a ratio of ~1 for p to s electrons in the Fe−N σ orbital, in contrast to the molecular orbital treatment which predicts a ratio of ~10 (Mun et al., 1979). We observe f_{2p}/f_{2s} ratios of ~0.2 and ~0.8 for N(1) and N(2), respectively, values which are consistent for the sp^n hybrid of an imidazole nitrogen (Scholes et al., 1982). These results are generally in good agreement with the values derived from the Q-band ENDOR data on the Rieske center of *P. cepacia* PDO [$f_{2p}/f_{2s} \sim 1$, for both N(1) and N(2)] and *R. capsulatus* bc_1 complex (Gurbiel et al., 1989, 1991).

In contrast to the values for N(1) and N(2), the much smaller A_{iso} value for N(3) can be compared with $A_{iso} \approx 1$ MHz measured for the ferredoxin class of [2Fe-2S] centers which are anchored to the protein by four cysteines (Cammack et al., 1988; Shergill & Cammack, 1994a; Dikanov et al., 1995). The weak hyperfine coupling might represent an interaction of the ferredoxin-type cluster through NH−S hydrogen bonds, as indicated in the protein structure (Fukuyama et al., 1980, 1995; Rypniewski et al., 1991). Alternatively, a long-distance exchange coupling to the cysteine α nitrogens cannot be excluded. It has been pointed out that NH−S hydrogen bonds are a possible factor for controlling the redox potential. However, it appears that the redox potential differences between dioxygenases and Rieske proteins cannot be ascribed to NH−S hydrogen bonds, as Rieske proteins also exhibit significant intensity in the 0−4.5 MHz region of ESEEM spectra (Britt et al., 1991; Shergill & Cammack, 1994b), which could be attributed to NH−S hydrogen-bonding interactions.

This work has demonstrated that 2D HYSCORE is a sensitive probe of electronic structure when applied to metal centers in proteins that show multiple couplings to nitrogen nuclei. *P. putida* ISP_{BED} has been cloned and overproduced (Butler, 1995), and these studies pave the way for future work on the effects of site-directed mutagenesis on the [2Fe-2S] cluster.

ACKNOWLEDGMENT

We dedicate this work to P. J. Geary (Shell Research Ltd., Shell Biosciences Laboratory, Sittingbourne Research Center, Sittingbourne, Kent, U.K.). We gratefully thank Mr. A. C. White (King's College, London) for technical assistance and Dr. P. Bratt (University College, London) for assistance and advice with the 2D ESEEM measurements.

REFERENCES

Ackrell, B. A. C., Kearney, E. B., Mims, W. B., Peisach, J., & Beinert, H. (1984) *J. Biol. Chem. 259*, 4015−4018.
Ashby, C. I. H., Cheng, C. P., & Brown, T. L. (1978) *J. Am. Chem. Soc. 100*, 6057−6063.
Atherton, N. M. (1973) *Electron Spin Resonance*, Wiley, New York.
Batie, C. J., Ballou, D. P., & Correll, C. J. (1991) in *Chemistry and Biochemistry of Flavoenzymes* (Muller, F., Ed.) pp 544−554, CRC Press, Boca Raton, FL.
Bertrand, P., Guigliarelli, B., Gayda, J. P., Beardwood, P., & Gibson, J. F. (1985) *Biochim. Biophys. Acta 831*, 261−266.
Britt, R. D., Sauer, K., Klein, M. P., Knaff, D. B., Krianciunas, A., Yu, C. A., Yu, L., & Malkin, R. (1991) *Biochemistry 30*, 1892−1901.
Butler, C. S. (1995) Ph.D. Thesis, King's College, University of London, U.K.
Cammack, R. (1992) in *Advances in Inorganic Chemistry - Iron-sulfur proteins* (Cammack, R., & Sykes, A. G., Eds.) Vol. 38, pp 281−322, Academic Press, San Diego.
Cammack, R., Chapman, A., McCracken, J., Cornelius, J. B., Peisach, J., & Weiner, J. H. (1988) *Biochim. Biophys. Acta 956*, 307−312.
Cline, J. F., Hoffman, B. M., Mims, W. B., LaHáie, E., Ballou, D. P., & Fee, J. A. (1985) *J. Biol. Chem. 260*, 3251−3254.
Crutcher, S. E., & Geary, P. J. (1979) *Biochem. J. 177*, 393−400.

Davidson, E., Ohnishi, T., Atta-Asafo-Adjei, E., & Daldal, F. (1992) *Biochemistry 31*, 3342−3351.
Dikanov, S. A., & Tsvetkov, Y. D. (1992) in *Electron Spin-echo Envelope Modulation (ESEEM) Spectroscopy*, pp 187−208, CRC Press, Boca Raton, FL.
Dikanov, S. A., Tyryshkin, A. M., Felli, I., Reijerse, E. J., & Hüttermann, J. (1995) *J. Magn. Reson., Ser. B 108*, 99−102.
Edmonds, D. T., & Speight, P. A. (1971) *Phys. Lett. 34A*, 325−326.
Fee, J. A., Findling, K. L., Yoshida, T., Hille, R., Tarr, G. E., Hearshen, D. O., Dunham, W. R., Day, E. P., Kent, T. A., & Munck, E. (1984) *J. Biol. Chem. 259*, 124−133.
Flanagan, H. L., & Singel, D. J. (1987) *J. Chem. Phys. 87*, 5606−5616.
Fukuyama, K., Hase, T., Matsumoto, S., Tsukihara, T., Katsube, Y., Tanaka, N., Kakudo, M., Wada, K., & Matsubara, H. (1980) *Nature 286*, 522−524.
Fukuyama, K., Ueki, N., Nakamura, H., Tsukihara, T., & Matsubara, H. (1995) *J. Biochem. 117*, 1017−1023.
Geary, P. J., Saboowalla, F., Patil, D. S., & Cammack, R. (1984) *Biochem. J. 217*, 667−673.
Geary, P. J., Mason, J. R., & Joannou, C. L. (1990) in *Methods in Enzymology*; *Hydrocarbons and Methylotrophy* (Lidstrom, M. E., Ed.) pp 52−60, Academic Press, San Diego.
Gemperle, C., Aebli, G., Schwieger, A., & Ernst, R. R. (1990) *J. Magn. Reson. 88*, 241.
Gibson, D. T., & Subramanian, V. (1984) in *Microbial Degradation of Organic Compounds* (Gibson, D. T., Ed.) pp 181−252, Marcel Dekker, New York.
Gibson, J. F., Hall, D. O., Thornley, J. H. M., & Whatley, F. R. (1966) *Proc. Natl. Acad. Sci. U.S.A. 56*, 987−990.
Graham, L. A., & Trumpower, B. L. (1991) *J. Biol. Chem. 266*, 22485−22492.
Gurbiel, R. J., Batie, C. J., Sivaraja, M., True, A. E., Fee, J. A., Hoffman, B. M., & Ballou, D. P. (1989) *Biochemistry 28*, 4861−4871.
Gurbiel, R. J., Ohnishi, T., Robertson, D. E., Daldal, F., & Hoffman, B. M. (1991) *Biochemistry 30*, 11579−11584.
Hatefi, Y., Haavik, A. G., & Griffiths, D. E. (1962a) *J. Biol. Chem. 237*, 1676−1680.
Hatefi, Y., Haavik, A. G., & Griffiths, D. E. (1962b) *J. Biol. Chem. 237*, 1680−1685.
Höfer, P. (1991) *Bruker Report 118*, 1−8.
Hoffman, B. M. (1991) *Acc. Chem. Res. 24*, 164−170.
Hoffman, B. M., Venters, R. A., & Martinsen, J. (1984a) *J. Magn. Reson. 59*, 110−123.
Hoffman, B. M., Venters, R. A., & Martinsen, J. (1984b) *J. Magn. Reson. 62*, 537−542.
Hoffman, B. M., DeRose, V. J., Doan, P. E., Gurbiel, R. J., Houseman, A. L. P., & Telser, J. (1993) in *Biological Magnetic Resonance 13: EMR of Paramagnetic molecules* (Berliner, L. J., & Reuben, J., Eds.) pp 151−218, Plenum Press, New York.
Hunt, M. J., & Mackay, A. L. (1976) *J. Magn. Reson. 22*, 295−301.
Jiang, F., Peisach, J., Ming, L.-J., Que, L., Jr., & Chen, V. J. (1991) *Biochemistry 30*, 11437−11445.
Kuila, D., Fee, J. A., Schoonover, J. R., Woodruff, W. H., Batie, C. J., & Ballou, D. P. (1987) *J. Am. Chem. Soc. 109*, 1559.
Kuila, D., Schoonover, J. R., Dyer, R. B., Batie, C. J., Ballou, D. P., Fee, J. A., & Woodruff, W. H. (1992) *Biochim. Biophys. Acta 1140*, 175.
LoBrutto, R., Haley, P. E., Yu, C. A., Ohnishi, T., & Leigh, J. S. (1986) *Biophys. J. 49*, 327a.
Lucken, E. A. C. (1969) in *Nuclear Quadrupole Coupling Constants*, pp 217−248, Academic Press, London.
Malkin, R., & Posner, H. B. (1978) *Biochim. Biophys. Acta 501*, 552−554.
Mason, J. R., & Cammack, R. (1992) *Annu. Rev. Microbiol. 46*, 277−305.
Mims, W. B. (1972a) *Phys. Rev. B5*, 2409−2419.
Mims, W. B. (1972b) *Phys. Rev. B6*, 3543−3545.
Mims, W. B., & Peisach, J. (1978) *J. Chem. Phys. 69*, 4921−4929.
Mims, W. B., & Peisach, J. (1981) in *Biological Magnetic Resonance* (Berliner, L. J., & Reuben, J., Eds.) p 213, Plenum Press, New York.
Mims, W. B., & Peisach, J. (1989) in *Advanced EPR, Applications in Biology and Biochemistry* (Hoff, A. J., Ed.) pp 1−57, Elsevier, Amsterdam.
Mun, S. K., Chang, J. C., & Das, T. P. (1979) *J. Am. Chem. Soc. 101*, 5562−5569.
Orme-Johnson, N. R., Mims, W. B., Orme-Johnson, W. H., Bartsch, R. G., Cusanovich, M. A., & Peisach, J. (1983) *Biochim. Biophys. Acta 748*, 68−72.
Rieske, J. S., McLennan, D. H., & Coleman, R. (1964a) *Biochem. Biophys. Res. Commun. 15*, 338−344.
Rieske, J. S., Zaugg, W. S., & Hansen, R. E. (1964b) *J. Biol. Chem. 239*, 3023−3030.
Rist, G. H., & Hyde, J. S. (1970) *J. Chem. Phys. 52*, 4633−4643.
Rypniewski, W. R., Breiter, D. R., Benning, M. W., Wesenberg, G., Oh, B.-H., Markley, J. L., Rayment, I., & Holden, H. (1991) *Biochemistry 30*, 4126−4131.
Scholes, C. P., Lapidot, A., Mascarenhas, R., Inubushi, T., Isaacson, R. A., & Feher, G. (1982) *J. Am. Chem. Soc. 104*, 2724−2735.
Schweiger, A. (1991) *Angew. Chem., Int. Ed. Engl. 30*, 265−292.
Shane, J. J., Höfer, P., Reijerse, E. J., & de Boer, E. (1992) *J. Mag. Res. 99*, 596−604.
Shergill, J. K., & Cammack, R. (1994a) *Biochim. Biophys. Acta 1185*, 43−49.
Shergill, J. K., & Cammack, R. (1994b) *Biochim. Biophys. Acta 1185*, 35−42.
Shergill, J. K., Weiner, J. H., & Cammack, R. (1991) *J. Chem. Soc., Faraday Trans. 87*, 3199−3202.
Shergill, J. K., Butler, C. S., White, A. C., Cammack, R., & Mason, J. R. (1994) *Biochem. Soc. Trans. 22*, 288.
Spiro, T. G. (1982) *Iron-Sulfur Proteins*, Wiley-Interscience, New York.
Tan, H.-M., Tang, H.-Y., Joannou, C. L., Abdel-Wahab, N. H., & Mason, J. R. (1993) *Gene 130*, 33−39.
Telser, J., Hoffman, B. M., LoBrutto, R., Ohnishi, T., Tsai, A. L., Simpkin, D., & Palmer, G. (1987) *FEBS Lett. 214*, 117−121.
Trumpower, B. (1981) *Biochim. Biophys. Acta 639*, 129−155.
van Camp, H. L., Sands, R. H., & Fee, J. A. (1981) *J. Chem. Phys. 75*, 2098−2107.

BI951826U